High-fidelity single-shot singlet-triplet readout of precision-placed donors in silicon

Article (Published Version)

High-Fidelity Single-Shot Singlet-Triplet Readout of Precision-Placed Donors in Silicon

M. A. Broome, T. F. Watson, D. Keith, S. K. Gorman, M. G. House, J. G. Keizer, S. J. Hile, W. Baker, and M. Y. Simmons

Centre of Excellence for Quantum Computation and Communication Technology, School of Physics, University of New South Wales, Sydney, New South Wales 2052, Australia

(Received 20 February 2017; published 25 July 2017)

In this work we perform direct single-shot readout of the singlet-triplet states in exchange coupled electrons confined to precision-placed donor atoms in silicon. Our method takes advantage of the large energy splitting given by the Pauli-spin blockaded (2,0) triplet states, from which we can achieve a single-shot readout fidelity of $98.4 \pm 0.2\%$. We measure the triplet-minus relaxation time to be of the order 3 s at 2.5 T and observe its predicted decrease as a function of magnetic field, reaching 0.5 s at 1 T.

DOI: 10.1103/PhysRevLett.119.046802

An increased ability to control and manipulate quantum systems is driving the field of quantum computation forward [1–4]. The spin of a single electron in the solid state has long been utilized in this context [5–11], providing a superbly clean quantum system with two orthogonal quantum states that can be measured with over 99% fidelity [12]. As a natural next step, the coupling of two electrons at separate sites has been studied in gate-defined quantum dots [5,13,14], as well as in donor systems [15–17]. In addition to being the eigenstates for two coupled spins, the singlet-triplet (ST) states of two electrons can form a qubit subspace, and have previously been utilized for quantum information processing [6,18–22]. Unlike in gate-defined quantum dots, donor systems do not require electrodes to confine electrons. The resulting decrease in physical complexity makes donor nanodevices very appealing for scaling up to many electron sites [15].

In the (1,1) charge configuration the ST states are eigenstates if the exchange coupling is greater than any difference in Zeeman energy between the two spins. The singlet and three triplet states are split only by the Zeeman energy in the cases of $|T^+\rangle = |\uparrow\uparrow\rangle$ and $|T^-\rangle = |\downarrow\downarrow\rangle$, and an exchange energy, J, for the singlet $|S\rangle = (|\uparrow\downarrow\rangle - |\downarrow\uparrow\rangle)/\sqrt{2}$ and $|T^0\rangle = (|\uparrow\downarrow\rangle + |\downarrow\uparrow\rangle)/\sqrt{2}$ states. However, in the (2,0) configuration all triplet states split from the singlet $|S(2,0)\rangle$ by a larger exchange interaction, Δ_{ST}, measured in previous works to be > 5 meV for donors [23]. The triplet states are therefore blocked from tunneling from the $(1,1) \rightarrow (2,0)$ charge configuration, known as Pauli spin blockade.

Typically, direct ST readout is performed by charge discrimination between the (1,1) and (2,0) states below the ST energy splitting Δ_{ST}. However, this relies on the charge sensor having a large enough differential capacitive coupling to each dot to discriminate between the two charge states. This is not possible in some architectures due to symmetry constraints, in particular, for donors it is advantageous for multiple donor sites to be coupled equally to a charge sensor for independent readout and/or loading. The tightly confined electron wave function at each donor site therefore necessitates that they are equidistant from the charge sensor. As a consequence $(1,1) \leftrightarrow (2,0)$ charge transfer signals are often too small to detect directly in this architecture.

Until now single-shot readout of ST states in donors has been limited to strongly coupled systems where the ST states comprise both the ground and excited valley-orbit states [17]. Furthermore, this method [17] has limited fidelity as it relies on spin dependent tunnel rates that cannot be independently controlled. Here we utilize an alternative technique to perform single-shot readout of ST states across two coupled donor sites in a regime suitable for quantum computing applications. Importantly, there is no need for any capacitive difference between the charge sensor and the two donor sites, as our method does not utilize a direct (1,1)-(2,0) charge transfer signal. Instead, we utilize an energy selective readout technique relying on relaxation of the metastable triplet state in the (1,1) configuration when pulsed into the (2,0) region. The method has been previously demonstrated in a time-averaged fashion [24–26]; however, we employ threshold discrimination analysis (cf., single-spin readout [27]) for single-shot readout with fidelity greater than 98%—close to fault tolerant thresholds for surface-code quantum computation [28].

The device shown in Fig. 1 was fabricated using scanning tunneling microscope hydrogen lithography. The patterned donor sites L and R consist of 2 and 1 phosphorus atoms, respectively, determined by examining the size of the lithographic patches [10,23] and their charging energies (see Supplemental Material [29]). Gates $\{G_L, G_M, G_R\}$ control electron numbers at L and R, whereas G_{SET} is predominantly coupled to the SET charge sensor. The SET is composed of approximately 1000 phosphorus atoms and is 19 ± 1 nm from L and R, allowing for electron loading and unloading; see Fig. 1(b). The SET is operated with a 2.5 mV source-drain bias and has a charging energy of ~5 meV. Further details of the fabrication methods have been published previously [30]. All data herein were taken inside a dilution refrigerator at 100 mK (electron temperature ~200 mK).

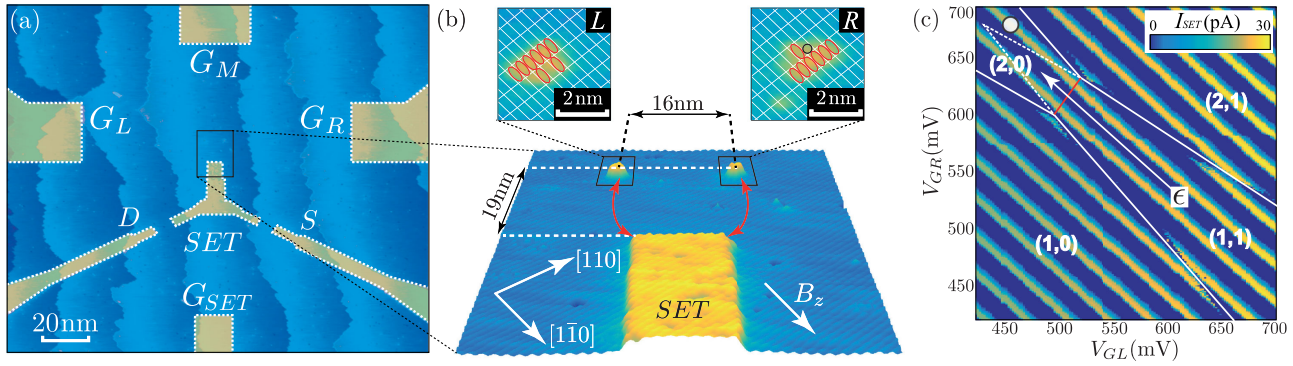

FIG. 1. The $(1,1) \leftrightarrow (2,0)$ charge transition in a double donor dot. (a) A scanning tunneling micrograph of the predosed device showing the hydrogen resist (blue region) and silicon beneath (yellow overlay). Three gates G_L, G_M, and G_R control the electrostatic environment of the donors dots. The single-electron transistor (SET) is tunnel coupled to source (S) and drain (D) and controlled predominantly by G_{SET}. (b) Donor sites L and R are separated by 16 ± 1 nm, and are equidistant at 19 ± 1 nm from a SET charge sensor, which also serves as an electron reservoir (red arrows). Insets are close-up images of L and R showing lithographic patches large enough for 2 and 1 P atoms respectively. (c) A charge stability map showing the current through the SET as a function of voltages $\{V_{GL}, V_{GR}\}$ near the (1,1)-(2,0) transition. Current peaks running at ~45° show Coulomb blockade of the SET and breaks in these lines correspond to single electron transitions of L and R. The solid white lines indicate the dot-SET ground-state transitions, whereas the area enclosed by the dashed white lines shows the region where $S(2,0)$ is the ground state and all $T(1,1)$ states are metastable. The detuning axis ϵ is shown by the white arrow. Singlet-triplet readout is performed at the point shown by the circle marker.

Figure 1(c) shows the SET current as a function of V_{GL} and V_{GR} near the (1,1)-(2,0) charge transition. No change in current is observed across the interdot transition (red line), and therefore ST readout cannot be performed here. Instead, we utilize two alternative tunneling routes to the $S(2,0)$ ground state near the (2,0)-(2,1) charge transition shown schematically in Fig. 2(a). Importantly, by monitoring the SET current in real time we can distinguish the two different tunneling routes. At the readout position [white circle marker in Fig. 1(c)] the SET current is high when electrons are in the (2,0) and low in the (2,1) charge state. When initializing here in a S(1,1) state, an electron on R can tunnel directly to L forming $S(2,0)$; because the SET is not sensitive to interdonor transitions no charge transfer signal is observed [see the left of Fig. 2(a)]. However, when initializing in any $T(1,1)$ state at the readout position, tunneling to $T(2,0)$ is prohibited due to Pauli-spin blockade [6,23,31,32]. Now the $S(2,0)$ ground state is reached via an

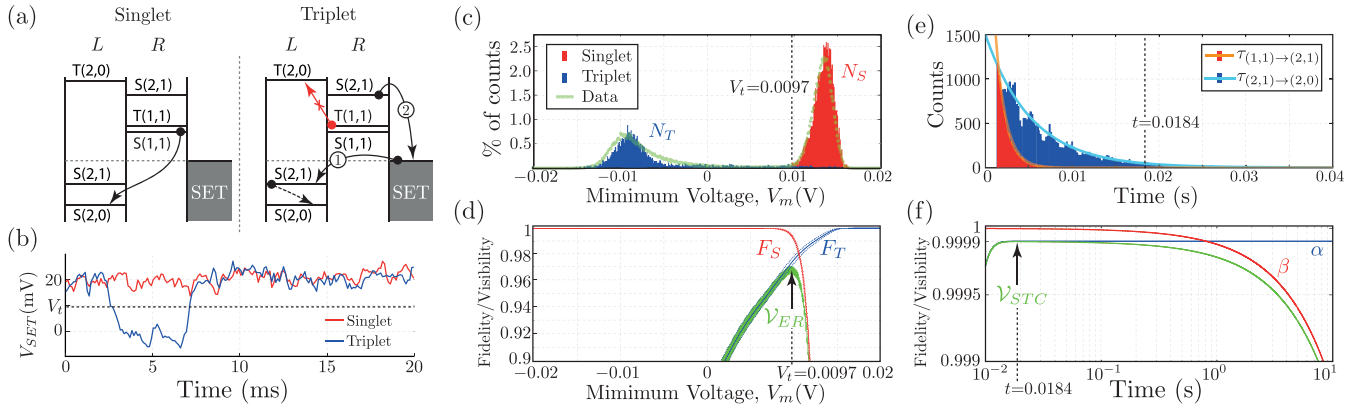

FIG. 2. Single-shot singlet-triplet readout in precision-placed donor atoms. (a) The relevant chemical potentials of electrons at donor sites L and R with respect to the SET Fermi level (grey region) at the readout position. The movement of electrons is shown by the solid black arrows and the red arrow depicts the forbidden transition of the $T(1,1)$ state to the $T(2,0)$ configuration due to Pauli-spin blockade. (b) Example SET readout trace of singlet and triplet states. [(c) and (d)] Optimization of electrical readout visibility, $\mathcal{V}_{\mathrm{ER}}$. Green markers in (c) show the minimum voltage after the current amplifier during readout for 100,000 traces. Solid bars show a simulation of 10,000 readout traces with a singlet (red) and triplet (blue) ratio of 1:2 as observed in the experiment. (d) The readout voltage threshold, V_t, is chosen to maximize $\mathcal{V}_{\mathrm{ER}}$ (green) based on individual readout fidelities for singlet (blue), F_S, and triplet (red), F_T, states. Shaded regions of each line indicate one standard deviation. [(e) and (f)] Optimization of state-to-charge conversion visibility, $\mathcal{V}_{\mathrm{STC}}$. (e) Experimentally obtained tunnel times (bars) for the relevant charge transitions and fits to exponential decays (lines). (f) State-to-charge conversion fidelities for triplet and singlet, α (blue) and β (red), respectively. Optimum readout time Δt gives the maximum visibility $\mathcal{V}_{\mathrm{STC}}$ (green). Analysis of ST readout was performed at $B_z = 2.5$ T, where T_1 of the $|T^-\rangle$ state is of the order of seconds.

electron first tunneling onto L to form (2,1) [singlet state on left donor site; see arrow ① in Fig. 2(a)] followed by an electron tunneling from R to the SET, forming the $S(2,0)$, shown by arrow ② in Fig. 2(a). This process results in a "dip" in SET current [27] that is used as the readout signal; see Fig. 2(b).

This charge transfer signal—given by movement of an electron to and from the SET—is as significant as for single-spin readout [10]. Furthermore, the large ST energy splitting Δ_{ST} for donors—much larger than in gate-defined quantum dots—is reproducible as it is not influenced by surrounding electrostatic gates [23]. The time scales for readout are dependent on the electron tunnel-on time from the SET to L, $\tau_{(1,1)\to(2,1)}$ [arrow ① in Fig. 2(a)], and tunnel-off time from R to the SET $\tau_{(2,1)\to(2,0)}$ [arrow ② in Fig. 2(a)]. These were determined by analyzing 100,000 readout traces to be $\tau_{(1,1)\to(2,1)} = 1.15 \pm 0.03$ ms and $\tau_{(2,1)\to(2,0)} = 5.3 \pm 0.2$ ms.

Following from previous works on single-shot spin readout [8–10,12,33], the assignment of singlet or triplet state to each readout trace comprises two separate parts, (i) electrical readout and (ii) state-to-charge conversion (STC), which we discuss in detail below.

(i) Electrical readout.—Here we determine whether a given SET current trace can be assigned as having a dip during the readout phase (time spent at the readout position), or not. In the experiment the SET current passes through a room temperature current amplifier; hence, the resulting voltage is relevant [see Fig. 2(b)]. During the readout phase a trace is assigned as having a voltage dip if its minimum value $V_m \leq V_t$. A Monte Carlo simulation of 10,000 readout traces with added white Gaussian noise equivalent to the experimental signal-to-noise ratio (SNR) is shown in Fig. 2(c) [9]. This histogram shows the simulated minimum voltages V_m from which we deduce the fidelity of assigning either a dip (triplet) or no dip (singlet), F_T or F_S, respectively, to each trace using the equations

$$F_T = 1 - \int_{V_t}^{\infty} N_T(V_m) dV_m \tag{1}$$

$$F_S = 1 - \int_{-\infty}^{V_t} N_S(V_m) dV_m, \tag{2}$$

where V_m is the minimum voltage and N_i is the fraction of each state i. The results are shown in Fig. 2(d) along with the calculated electrical readout visibility $\mathcal{V}_{\mathrm{ER}} = F_T + F_S - 1$. From Eqs. (1) and (2) we specify the optimum voltage threshold, V_t, where $\mathcal{V}_{\mathrm{ER}}$ is maximized. In total, 500 independent simulations were run (each 10,000 simulated traces) allowing the assignment of errors shown in Table I.

(ii) State-to-charge conversion.—Next we determine the optimum readout time, Δt, following the work on single-shot spin readout in [10,12]. The rate equation model described therein accounts for errors caused by relaxation of excited states, triplet states failing to cause a tunneling event before Δt, and a singlet state causing a tunneling event within Δt. As inputs to the model, the tunneling out time of the triplet state from $(1,1) \to (2,1)$, $\tau_{T,\mathrm{out}}$ is assigned the same value as $\tau_{(1,1)\to(2,1)}$, as shown in Fig. 2(e). The tunnel time, $\tau_{S,\mathrm{out}}$, is also found experimentally by counting the number of tunneling events occurring after a time much greater than $\tau_{T,\mathrm{out}}$ (here we used 8 ms) and attributing them to the exponential decay of the singlet state. Only 0.033% of the 100,000 readout traces showed tunneling after this time, giving an estimate of $\tau_{S,\mathrm{out}} = 16600 \pm 8300$ s. Using these characteristic tunneling times, we implement a rate equation model to determine the optimum readout time [10], Δt, based on the probability of successfully assigning a voltage dip a triplet or singlet state, α and β, respectively (see Supplemental Material [29]).

TABLE I. Parameters for singlet-triplet readout.

Electrical readout	Value	STC conversion	Value
V_t (V)	0.0097 ± 0.0007	Δt (ms)	18.4 ± 0.7
F_S (%)	99.4 ± 0.1	$\alpha(\%)$ (%)	99.990 ± 0.001
F_T (%)	97.3 ± 0.3	β (%)	99.999 ± 0.001
$\mathcal{V}_{\mathrm{ER}}$ (%)	96.8 ± 0.3	$\mathcal{V}_{\mathrm{STC}}$ (%)	99.989 ± 0.001

The resulting assignment probabilities α and β are shown as a function of the readout time in Fig. 2(f). Similar to electrical readout, the visibility of state-to-charge conversion is calculated as $\mathcal{V}_{\mathrm{STC}} = \alpha + \beta - 1$, and the optimum readout time is chosen where $\mathcal{V}_{\mathrm{STC}}$ is maximized and was found to be $\Delta t = 18.4 \pm 0.7$ ms.

Table I gives a summary of the fidelity calculations, where the final measurement fidelity is given by $F_M = (\alpha F_T + \beta F_S)/2 = 98.4 \pm 0.2\%$. Owing to the large energy separation between the $S(2,0)$ and $T(2,0)$ states, thermal broadening of the Fermi distribution in the SET ($T_e = 200$ mK) has a negligible effect on the readout fidelity. As such, the $\mathcal{V}_{\mathrm{STC}}$ is reported very close to unity.

For this device the ST readout fidelity was limited by low electrical visibility $\mathcal{V}_{\mathrm{ER}}$, itself restricted by a relatively low SET peak current of 30 pA. Here we have a signal-to-noise ratio of 6.4, but with an increase of SET signal equivalent to SNR = 8, we estimate achieving fidelities > 99%. Single-shot charge detection of this quality has previously been demonstrated in donor systems using dc-biased SETs [12,15] and with rf reflectometry, which significantly improves SNR further still [34]. Nonetheless, high-fidelity ST readout can be maintained over a large range of magnetic fields—as demonstrated in Fig. 3(d)—because Δ_{ST} is independent of B_z.

Singlet-triplet dynamics.—As a demonstration of this readout technique, here we map out the $|S(2,0)\rangle \leftrightarrow |T^-\rangle$ anticrossing as a function of B_z. Figure 3(a) shows the two electron eigenspectrum with the addition of the $|S(2,0)\rangle$ state as a function of detuning, ϵ [see the arrow in Fig. 1(c)]. To observe ST mixing we initialize deterministically in

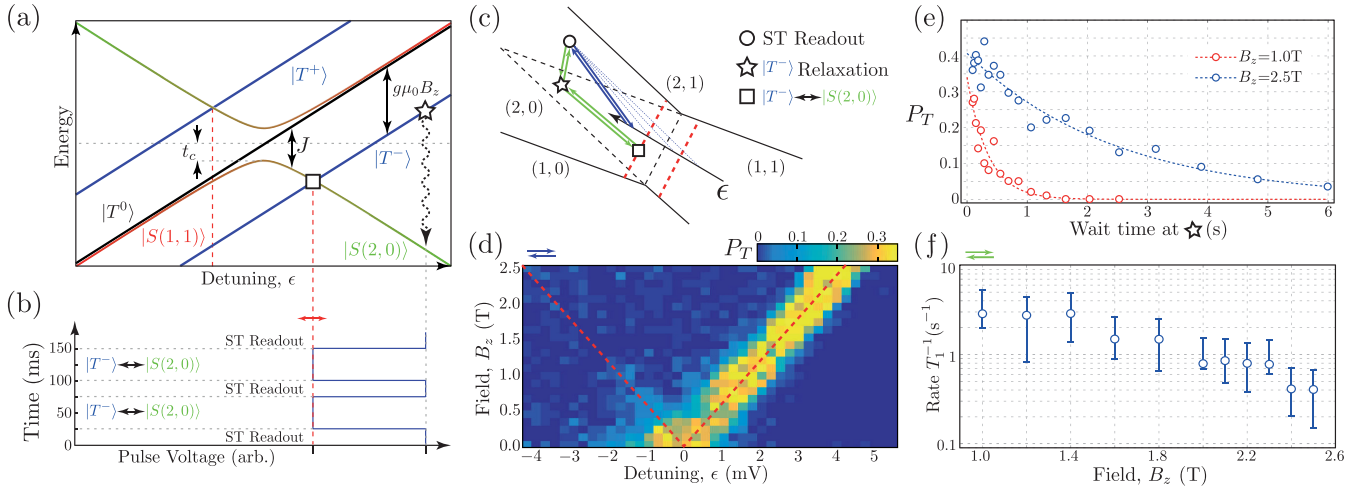

FIG. 3. Field dependence of $|S(2,0)\rangle \leftrightarrow |T^-\rangle$ mixing and $|T^-\rangle T_1$ relaxation. (a) The eigenspectrum of the two electron system at the (1,1)-(2,0) charge transition in a static magnetic field B_z. The detuning parameter ϵ corresponds to the black arrow shown in (c), and controls the exchange coupling, J, between the electrons. (b) A schematic of the two-level pulse scheme used to observe mixing between $|S(2,0)\rangle \leftrightarrow |T^-(1,1)\rangle$ states. (c) Pulsing schemes for results shown in [(d)–(f)]. (d) The triplet probability, P_T, as a function of static magnetic field B_z and the wait position along the detuning axis, ϵ. A peak at 45° for $\epsilon > 0$ corresponds to the position in this parameter space where mixing between $|S(2,0)\rangle \leftrightarrow |T^-(1,1)\rangle$ can occur. A fainter peak running at −45° in the data corresponds to $|S(2,0)\rangle \leftrightarrow |T^+(1,1)\rangle$ mixing for $\epsilon < 0$. [(e) and (f)] Measurement of the $|T^-\rangle T_1$ time. To initialize the $|T^-\rangle$ state we wait at a position along ϵ shown by the square marker in (a) and (c) that follows the dotted red line in (d) for $\epsilon > 0$ as a function of field, B_z. (e) Probability of the triplet state for $B_z = \{1.0, 2.5\}$ T, as a function of the time spent at the star marker shown in (c). (f) Measurement of T_1 from $B_z = 1.0 \rightarrow 2.5$ T.

$|S(2,0)\rangle$ by performing ST readout. Next we apply a 50 ms pulse along the detuning axis toward the $|S(2,0)\rangle \leftrightarrow |T^-\rangle$ anticrossing, allowing sufficient time for mixing [see Fig. 3(b)]. Two of the triplet states $\{|T^+\rangle, |T^-\rangle\}$ are split by the Zeeman energy from the $|S(1,1)\rangle$ and $|T^0\rangle$ states, such that the position mixing between $|S(2,0)\rangle \leftrightarrow \{|T^-\rangle, |T^+\rangle\}$ changes with B_z. The two-level pulse scheme is shown schematically by the blue arrows in Fig. 3(c) along with the ST mixing positions shown by the red dashed lines (not to scale). Finally, we pulse back to the ST readout position (circle marker) for 25 ms where we measure the triplet state probability; the results are shown in Fig. 3(d).

In addition to a clear $|S(2,0)\rangle \leftrightarrow |T^-\rangle$ mixing point for $\epsilon > 0$, indicated by the high triplet probability in Fig. 3(d) (yellow), a faint feature related to $|S(2,0)\rangle \leftrightarrow |T^+\rangle$ mixing can also be seen at detuning values $\epsilon < 0$. Mixing between $|S(2,0)\rangle \leftrightarrow |T^+\rangle$ is suppressed due to fast charge relaxation from $|S(2,0)\rangle \rightarrow |S(1,1)\rangle$ in this region. The position of $|S(2,0)\rangle \leftrightarrow |T^-\rangle$ mixing in ϵ remains linear as a function of B_z, indicating a small value of tunnel coupling [t_c in Fig. 3(a)], and hence no spin-funnel shape is seen as reported in similar experiments [14,33].

Finally, using the $|S(2,0)\rangle \leftrightarrow |T^-\rangle$ mixing point to randomly load the $|T^-\rangle$ state, we measure its T_1 lifetime using the three-level pulsing protocol shown by the green arrows in Fig. 3(c). Relaxation of the $|T^-\rangle$ state occurs while inside the charge region enclosed by the dashed lines in Fig. 3(c), i.e., where only interdonor-site tunneling is allowed. This position, indicated by the star marker in Fig. 3(c), lies at $\epsilon = 10$ mV, ensuring that $|S(2,0)\rangle$ remains the ground state for $B_z \leq 2.5$ T. The results for T_1 are shown in Figs. 3(e) and 3(f). The observed decrease in $1/T_1$ as a function of increasing B_z follows as a result of the decreasing energy gap between the excited $|T^-\rangle$ state and $|S(2,0)\rangle$ ground state [35]. Previous theoretical studies of triplet state relaxation in donors coupled along [001] predict a dependence on exchange energy as approximately, $1/T_1 \sim J^3$ [35], and should be the focus of future experimental work.

High-fidelity single-shot readout of individual and multiple qubit states is a prerequisite for the observation of postclassical multiqubit phenomena, in particular, two-qubit entanglement [1]. In the original Kane proposal for scalable donor-based quantum computing architectures, the single-shot measurement of ST states is suggested to facilitate the readout of nuclear spins [36] and is advantageous over previously used readout techniques [37] as it does not require the high-frequency manipulation of the electron spin. Furthermore, ST readout can be used to measure single-electron spin qubits [13] at lower magnetic fields and higher temperatures easing the constraints on microwave electronics and cryogenic cooling [38]. Finally, encoding qubits using ST states [21,39,40] allows for an all electrical approach for control; in particular, multiple qubits can be coupled by utilizing the inherent electric dipole coupling given by the (1,1)-(2,0) charge configurations [41,42]. The results obtained herein, in addition to the reduced complexity of electron confinement in donors, make a compelling case for further research on the scaling

of multiple forms of donor-based quantum computing architectures.

This research was conducted by the Australian Research Council Centre of Excellence for Quantum Computation and Communication Technology (Grant No. CE110001027) and the U.S. National Security Agency and U.S. Army Research Office (Contract No. W911NF-08-1-0527). M. Y. S. acknowledges an ARC Laureate Fellowship.

[1] M. A. Nielsen and I. L. Chuang, *Quantum Computation and Quantum Information* (Cambridge University Press, Cambridge, 2010).
[2] T. D. Ladd, F. Jelezko, R. Laflamme, Y. Nakamura, C. Monroe, and J. L. O'Brien, Nature (London) **464**, 45 (2010).
[3] I. M. Georgescu, S. Ashhab, and F. Nori, Rev. Mod. Phys. **86**, 153 (2014).
[4] B. M. Terhal, Rev. Mod. Phys. **87**, 307 (2015).
[5] J. R. Petta, A. C. Johnson, C. M. Marcus, M. P. Hanson, and A. C. Gossard, Phys. Rev. Lett. **93**, 186802 (2004).
[6] A. C. Johnson, J. R. Petta, J. M. Taylor, A. Yacoby, M. D. Lukin, C. M. Marcus, M. P. Hanson, and A. C. Gossard, Nature (London) **435**, 925 (2005).
[7] R. Hanson, L. P. Kouwenhoven, J. R. Petta, S. Tarucha, and L. M. K. Vandersypen, Rev. Mod. Phys. **79**, 1217 (2007).
[8] J. J. Pla, K. Y. Tan, J. P. Dehollain, W. H. Lim, J. J. L. Morton, D. N. Jamieson, A. S. Dzurak, and A. Morello, Nature (London) **489**, 541 (2012).
[9] A. Morello *et al.*, Nature (London) **467**, 687 (2010).
[10] H. Buch, S. Mahapatra, R. Rahman, A. Morello, and M. Y. Simmons, Nat. Commun. **4**, 2017 (2013).
[11] T. F. Watson, B. Weber, J. A. Miwa, S. Mahapatra, R. M. P. Heijnen, and M. Y. Simmons, Nano Lett. **14**, 1830 (2014).
[12] T. F. Watson, B. Weber, M. G. House, H. Büch, and M. Y. Simmons, Phys. Rev. Lett. **115**, 166806 (2015).
[13] F. H. L. Koppens, C. Buizert, I. T. Vink, K. C. Nowack, T. Meunier, L. P. Kouwenhoven, and L. M. K. Vandersypen, J. Appl. Phys. **101**, 081706 (2007).
[14] B. M. Maune *et al.*, Nature (London) **481**, 344 (2012).
[15] T. F. Watson, B. Weber, H. Büch, M. Fuechsle, and M. Y. Simmons, Appl. Phys. Lett. **107** (2015).
[16] M. G. House, T. Kobayashi, B. Weber, S. J. Hile, T. F. Watson, J. van der Heijden, S. Rogge, and M. Y. Simmons, Nat. Commun. **6** (2015).
[17] J. P. Dehollain, J. T. Muhonen, K. Y. Tan, A. Saraiva, D. N. Jamieson, A. S. Dzurak, and A. Morello, Phys. Rev. Lett. **112**, 236801 (2014).
[18] J. R. Petta *et al.*, Science **309**, 2180 (2005).
[19] J. M. Taylor, J. R. Petta, A. C. Johnson, A. Yacoby, C. M. Marcus, and M. D. Lukin, Phys. Rev. B **76**, 035315 (2007).
[20] J. R. Prance *et al.*, Phys. Rev. Lett. **108**, 046808 (2012).
[21] E. A. Laird, J. M. Taylor, D. P. DiVincenzo, C. M. Marcus, M. P. Hanson, and A. C. Gossard, Phys. Rev. B **82**, 075403 (2010).
[22] D. Kim, D. R. Ward, C. B. Simmons, D. E. Savage, M. G. Lagally, M. Friesen, S. N. Coppersmith, and M. A. Eriksson, npj Quantum Inf. **1**, 15004 EP (2015).
[23] B. Weber, Y. H. Matthias Tan, S. Mahapatra, T. F. Watson, H. Ryu, R. Rahman, L. C. L. Hollenberg, G. Klimeck, and M. Y. Simmons, Nat. Nanotechnol. **9**, 430 (2014).
[24] S. A. Studenikin, J. Thorgrimson, G. C. Aers, A. Kam, P. Zawadzki, Z. R. Wasilewski, A. Bogan, and A. S. Sachrajda, Appl. Phys. Lett. **101** (2012).
[25] J. D. Mason, S. A. Studenikin, A. Kam, Z. R. Wasilewski, A. S. Sachrajda, and J. B. Kycia, Phys. Rev. B **92**, 125434 (2015).
[26] P. Harvey-Collard *et al.*, arXiv:1512.01606.
[27] J. M. Elzerman, R. Hanson, L. H. Willems van Beveren, B. Witkamp, L. M. K. Vandersypen, and L. P. Kouwenhoven, Nature (London) **430**, 431 (2004).
[28] A. G. Fowler, M. Mariantoni, J. M. Martinis, and A. N. Cleland, Phys. Rev. A **86**, 032324 (2012).
[29] See Supplemental Material at http://link.aps.org/supplemental/10.1103/PhysRevLett.119.046802 for details about (1) the derivation and calculation of charging energies for the donor dots L and R, (2) concerns the derivation of state-to-charge conversion.
[30] A. Fuhrer, M. Fuechsle, T. C. G. Reusch, B. Weber, and M. Y. Simmons, Nano Lett. **9**, 707 (2009).
[31] K. Ono, D. G. Austing, Y. Tokura, and S. Tarucha, Science **297**, 1313 (2002).
[32] F. H. L. Koppens, C. Buizert, K. J. Tielrooij, I. T. Vink, K. C. Nowack, T. Meunier, L. P. Kouwenhoven, and L. M. K. Vandersypen, Nature (London) **442**, 766 (2006).
[33] M. Veldhorst *et al.*, Nature (London) **526**, 410 (2015).
[34] M. G. House, I. Bartlett, P. Pakkiam, M. Koch, E. Peretz, J. vanderHeijden, T. Kobayashi, S. Rogge, and M. Y. Simmons, Phys. Rev. Applied **6**, 044016 (2016).
[35] M. Borhani and X. Hu, Phys. Rev. B **82**, 241302 (2010).
[36] B. E. Kane, Nature (London) **393**, 133 (1998).
[37] J. J. Pla, K. Y. Tan, J. P. Dehollain, W. H. Lim, J. J. L. Morton, F. A. Zwanenburg, D. N. Jamieson, A. S. Dzurak, and A. Morello, Nature (London) **496**, 334 (2013).
[38] L. Vandersypen *et al.*, arXiv:1612.05936.
[39] D. Kim *et al.*, Nature (London) **511**, 70 (2014).
[40] X. Wu, PhD thesis, The University of Wisconsin-Madison, 2015.
[41] M. D. Shulman, O. E. Dial, S. P. Harvey, H. Bluhm, V. Umansky, and A. Yacoby, Science **336**, 202 (2012).
[42] J. M. Nichol, L. A. Orona, S. P. Harvey, S. Fallahi, G. C. Gardner, M. J. Manfra, and A. Yacoby, npj Quantum Inf. **3**, 3 (2017).